COMMUNICATIONS IN SCIENCE AND TECHNOLOGY
Homepage: cst.kipmi.or.id

Investigating the antimicrobial activity of silver nanoparticles with varying charges green-synthesized from *Tabebuia rosea* flower

Trung Dien Nguyen*, Thao Phuc-Nguyen Nguyen, Nhung Thi-Tuyet Thai, Yen Hai Hoang, Gia Thi-Ngoc Trinh

School of Education, Can Tho University, 94000, Vietnam

Article history:
Received: 1 September 2024 / Received in revised form: 9 December 2024 / Accepted: 11 December 2024

Abstract

The integration of nanotechnology and biomedicine has driven a significant interest in silver nanoparticles due to their unique properties. This study presents a novel approach by combining *Tabebuia rosea* flower extract and chitosan to manipulate the surface charges of synthesized silver nanoparticles. These biosynthesized nanoparticles, presenting negative, neutral, and positive charges, were thoroughly analyzed by means of a number of techniques including Ultraviolet-visible spectroscopy, X-ray diffraction, transmission electron microscopy, and Fourier-transform infrared spectroscopy. By incorporating chitosan, the zeta potential of the green-synthesized nanomaterials was modified, shifting from negative to positive. The resultant silver nanoparticles showed the zeta potentials of –24.8 mV for negatively charged particles, +22.9 mV for positively charged ones, and neutrality at approximately 0.04% chitosan. Meanwhile, the particle sizes for the negative, neutral, and positive nanomaterials were 19.7, 15.8, and 14.2 nm, respectively. The antimicrobial and anticancer activities of these biosynthesized nanoparticles were evaluated against gram-negative bacteria (*Pseudomonas aeruginosa*, *Escherichia coli*, and *Salmonella enterica*), gram-positive bacteria (*Bacillus subtilis*, *Lactobacillus fermentum*, and *Staphylococcus aureus*), and cancer cell lines (A549, Hep-G2, KB, and MCF-7). These results highlight the crucial role of surface stabilizers, particle size, and charge in determining the biomedical potential of nanosilver particles. Notably, the biosynthesized silver nanoparticles exhibited a number of promising antimicrobial and anticancer properties, emphasizing their potential for biomedical applications.

Keywords: Anticancer activity, antimicrobial properties, chitosan, silver nanoparticles, *Tabebuia rosea* flower

1. Introduction

The realm of nanotechnology has unfurled a panorama of possibilities, particularly within the sphere of biomedicine, leveraging the exceptional attributes of nanoparticles. Silver nanoparticles (AgNPs) have emerged as the focal points of extensive exploration in view of their remarkable biological characteristics. These nanoscale entities exhibit potent antibacterial, antifungal, and anticancer properties, positioning them as promising contenders for biomedical applications [1,2]. The negative-charged nanoparticles of 10-30 nm spherical shape were biosynthesized by *Syzygium nervosum* bud extract as both reductants and stabilizers. The obtained nanomaterials exhibited a high inhibition for *Staphylococcus aureus*, *Bacillus subtilis*, *Salmonella Typhi*, and *Escherichia coli* [3]. *Azadirachta indica* fruit extract is beneficial for the AgNPs bio-synthesis owing to the presence of polyphenols, flavonoids, and tannins. The naturally produced AgNPs states a negative charge with a zeta potential of −36 mV. The as-prepared AgNPs substantially suppressed the lung cancer A549 cell line [4]. Another study on *Melia azedarach* leaf-assisted synthesis for AgNPs was conducted at ambient conditions in which the negatively charged spherical particles with a size range of 18-30 nm efficiently inhibited the *Verticillium dahlia* growth [5]. However, most studies have concentrated on the synthesis of negatively charged AgNPs more, but on positively charged AgNPs less.

In synthesizing the positive-charged AgNPs, the choice of stabilizing agents assumes pivotal importance in determining their properties. Of the diverse agents investigated, achieving and maintaining a positively charged state for AgNPs has shown the enhanced stability and reactivity, albeit presenting challenges [6,7]. Notably, the synthesis process, influenced by factors such as pH alterations, significantly impacts the charge of chemicals employed in both human-mediated synthesis and natural plant extract methodologies [8,9]. Various studies have examined different agents, each with distinct advantages and limitations. The challenge, however, persists in creating nanoparticles that are diminutive in size and possess a substantial zeta potential, even when leveraging the eco-friendly advantages of natural plant extracts [10,11]. Pokhrel et al. synthesized the positive-charged AgNPs with a particle size of approximately 5 nm and a zeta potential of +42 mV.

* Corresponding author.
Email: ndtrung@ctu.edu.vn
https://doi.org/10.21924/cst.9.2.2024.1521

The synthesis process used $AgNO_3$ precursors, $NaBH_4$ reducing agent, and stabilizers to create the positive charges: ethyleneimine C_2H_5N and N-(2-hydroxyethyl)piperazine-N′-(2-ethane sulfonic) acid $C_8H_{18}N_2O_4S$. The positive-charged nanomaterials were formed through the reduction of sodium borohydride $NaBH_4$ for 6 hours under UV irradiation [12]. Meanwhile, AgNPs with positive charges were synthesized from the reducing agent sodium borohydride $NaBH_4$ and the surface charge generating agent 1-dodecyl-3-methylimidazolium chloride $C_{16}H_{31}ClN_2$ in chlorhexidine (CHX) solvent $C_{22}H_{30}Cl_2N_{10}$. The zeta potential distribution diagram showed two potentials: +18 mV for $AgNPs^+$ and +56 mV for $CHXAgNPs^+$ [13]. Another stabilizer that formed positive charges-cysteamine hydrochloride was studied. A zeta potential being to +58 mV of the fabricated AgNPs was prepared by mixing sodium borohydride $NaBH_4$ and cysteamine hydrochloride C_2H_8ClNS [14]. By entering chitosan, a natural polysaccharide has surfaced as an effective stabilizer in the synthesis of AgNPs. Through the integration of chitosan, it becomes possible to regulate the surface charge of AgNPs, surmounting instability issues and ensuring controlled properties amenable to diverse biomedical applications [15,16]. Chitosan is known as a biodegradable polymer with the presence of amino ($-NH_2$) and hydroxyl (-OH) groups in its structure. This is favorable for protecting metallic nanoparticles and forming positive charges on the nanoparticle surface by renovating glucosamine units' acidification to the soluble protonated structure NH_3^+ [17]. According to Cinteza, the presence of chitosan significantly varied the zeta potential of the synthesized AgNPs to shift from –11.2 to +75 mV [18].

Besides the positive charge-generating stabilizers, the friendly-environmental reducing agents are also of interest for synthesizing metallic nanoparticles. Reducing agents present in plant extracts have recently been recognized as a useful resource for metallic nanosynthesis [19]. Within the synthesis methodology using plant extract, the chemical composition of species such as the Rosy Trumpet flowers (*Tabebuia rosea* or *T. rosea*) holds a significant intrigue for its potential in nanoparticle synthesis. The analyses of the chemical constituents within *T. rosea* flowers, originating from Latin American countries, revealed a plethora of useful compounds. In particular, terpenoids, steroids, flavonoids, tannins, and phenolic compounds exhibit robust antioxidant properties, rendering them suitable as both reducing and capping agents [20,21]. Compared to other plant extracts, *T. rosea* flowers possess a chemical composition particularly conducive to AgNPs synthesis. However, research utilizing *T. rosea* flower extract for synthesizing AgNPs, to best of our knowledge, remains limited still. This highlights the novelty of the present study, seeking to diversify the range of plant extracts used in nanomaterial synthesis while taking advantage of the abundant, low-cost, and readily available natural resources. The investigation and utilization of *T. rosea* flowers not only contribute to expanding the application of plant extracts in nanoscience but also foster the development of eco-friendly, green synthesis methods in the pharmaceutical and biomedical industries.

This study embarks on a pioneering synthesis approach, harnessing extracts derived from *T. rosea* flowers to fabricate AgNPs, denoted as AgNPsTr. Moreover, the integration of chitosan into this synthesis process aims not only to stabilize but also to finely modulate the surface charge and zeta potential of AgNPsTr. The use of eco-friendly *T. rosea* flower extract and the biodegradable stabilizer chitosan, instead of the toxic $NaBH_4$ and hard-to-degrade commercial stabilizers, is an innovative approach in this study compared to previous research on synthesizing positively charged AgNPs. By assessing the antibiotic activity of AgNPsTr against diverse microorganisms, considering three distinct charges of zeta potential - negative, neutral, and positive - critical insights into the influence of the surface charge, particle size, and stabilizer on their biomedical efficacy will be elucidated.

2. Materials and Methods

2.1. Materials

The chemicals utilized in the production and characterization of AgNPs were provided by Sigma-Aldrich. Silver nitrate $AgNO_3$ was employed as the primary precursor, while the extract derived from the *T. rosea* flowers was utilized both as a reducing agent and as a stabilizing agent in the synthesis of AgNPs. Additionally, a solution containing chitosan $C_{56}H_{103}N_9O_{39}$ dissolved in ascorbic acid $C_6H_8O_6$ was introduced as an auxiliary capping agent purposely to modulate the properties of the synthesized AgNPs.

2.2. Preparing the extract

T. rosea flowers were gathered on the premises of Can Tho University, subsequently desiccated, and processed into a powdered form. This powder was then subjected to a stirring and heating process in distilled water purposely to extract the desired components. For optimization, the temperature and duration of the extraction process were systematically adjusted.

2.3. Synthesizing AgNPs-Neg

$AgNO_3$ was introduced into various extract solutions and subjected to stirring to generate AgNPs. The nanoparticles synthesized under the most favorable conditions within the extract solution were labeled as AgNPs-Neg. The optimization process involved the adjustment of operational parameters, encompassing the quantities of *T. rosea* flower extract (0.6, 0.9, 1.2, 1.5, and 1.8 g L^{-1}), extraction temperature (40, 50, 60, 70, and 80°C), and extraction duration (10, 20, 30, 40, and 50 min).

2.4. Synthesizing AgNPs-Neu and AgNPs-Pos

The process involved the dissolution of ascorbic acid in the *T. rosea* flower extract for preparing optimal conditions, and ensuring a specific ascorbic acid concentration of 100 mM to yield solution X. Having prepared the formulation of solution X, chitosan was incorporated into this solution, considering a range of chitosan concentrations, specifically 0.08, 0.16, 0.24, and 0.32%. This process produced the discrete AgNPs variants. The diverse chitosan concentrations were associated

with distinct zeta potentials manifested in the resultant AgNPs. From the results of the relationship between zeta potential and chitosan concentration, the chitosan concentration for the AgNPs surface with positive (designated as AgNPs-Pos) and neutral charge (denoted as AgNPs-Neu) was determined.

2.5. Analyzing characteristics

To assess the formation of AgNPs, the examination of the 300-700 nm wavelength range was conducted by operating UV-Vis spectrophotometry (V730, Jasco). The zeta potential of the resultant AgNPs was then determined using an SZ-100 nanoparticle analyzer. To gauge the efficiency of the synthesis process, samples were subjected to an analysis of Ag^+ ion concentration through inductively coupled plasma optical emission spectroscopy (ICP-OES). This evaluation encompassed both the initial solution, comprising only the $AgNO_3$ precursor, and the resultant AgNPs solution. Prior to carry out an analysis, the AgNPs solution was centrifugated at 6500 rpm-4 h to eliminate any solid components. The synthesis efficiency, expressed as SE, was calculated through the formula (1).

(1)

where $C_{Ag,ini}$ represents the Ag^+ concentration of the initial solution and $C_{Ag,fin}$ signifies the Ag^+ concentration of the resulting solution.

For morphological analysis, transmission electron microscopy (TEM) with a Jem-1400 (Jeol) instrument was employed. Here, ImageJ software was used to determine the size distribution of the generated AgNPs. The materials' chemical compositions and functional groups were examined with the aid of a Thermo Nicolet 6700 Fourier transform infrared (FTIR) spectrometer. The crystalline phase of the extract-assisted production was confirmed through X-ray diffraction (XRD) with a Bruker D2 Phaser, equipped with Cu Kα radiation (40 mA, 40 kV). Diffracted intensities were measured over a range of 10 to 80° of 2θ angles. The average crystallite size of the synthesized AgNPs was estimated using Debye Scherrer's formula (2).

(2)

where Cry represents the crystal size, α indicates the full width at half maximum (Fw), θ represents Bragg's angle measured in radians, and Wa denotes the X-ray wavelength.

2.6. Assessing antimicrobial activities

A range of bacterial and fungal strains were employed to assess antimicrobial properties. For testing positive gram reactions, *Bacillus subtilis* (*B. subtilis,* ATCC 6633), *Lactobacillus fermentum* (*L. fermentum,* N4), and *Staphylococcus aureus* (*S. aureus,* ATCC 12600) were utilized. Whereas, for testing negative ones, the strains *Escherichia coli* (*E. coli,* ATCC 25922), *Pseudomonas aeruginosa* (*P. aeruginosa,* ATCC 15442), and *Salmonella enterica* (*S. enterica,* ATCC 35664) were included. The assessment of antibacterial activity was carried out through the broth microdilution method. To achieve a concentration of 5×10^5 colony-forming units per milliliter (CFU mL^{-1}), pathogenic cultures were subcultured and incubated at 37°C-24 h based upon MacFarland's standard guidelines. Ampicillin served as the control for positive gram bacteria, cefotaxime for negative gram bacteria, and nystatin for fungi. The determination of the IC_{50} value, representing the concentration at which 50% inhibition occurred, for the synthesized AgNPs-Neg, AgNPs-Neu, and AgNPs-Pos was conducted using 96-well microplates with absorbance measurements recorded at 630 nm.

2.7. Assessing antiproliferative activities

The antiproliferative impact of the synthesized AgNPs-Neg, AgNPs-Neu, and AgNPs-Pos was assessed across the range of cancer cell lines, which encompassed A549 (lung cancer), Hep-G2 (hepatic cancer), KB (epidermal carcinoma), and MCF-7 (breast cancer). These cell lines were subcultured in Dulbecco's modified Eagle's medium (DMEM), fortified with 10% fetal bovine serum (FBS) and 1% penicillin-streptomycin, and maintained in a 5% CO_2 incubator. For evaluating cell viability, trypan blue staining was conducted, and viable cell counts were performed by means of a hemocytometer. The cancer cell density was standardized to 3×10^4 colony-forming units per milliliter (CFU mL^{-1}), and the cell suspension was introduced into a 96-well plate for a 72-hour incubation period. To appraise the antiproliferative effect of AgNPs-Neg, AgNPs-Neu, and AgNPs-Pos, A549, Hep-G2, KB, and MCF-7 cell lines were subjected to the different concentrations of 32, 129, 516, and 2065 mg L^{-1} with dimethyl sulfoxide (DMSO) serving as the dilution agent. Following a 72-hour incubation in a 5% CO_2 environment, MTT reagent at a concentration of 100 mg/mL was introduced and incubated at 37°C-4 h. Formazan was subsequently solubilized using 100µL of DMSO, and absorbance measurements were taken at 540 nm in a 96-well plate. The reference sample used in this study was ellipticine. The percentage of cell growth inhibition was computed by using the formula (3).

(3)

where I signifies the cell growth inhibition percentage. For the blank, control, and tested samples, the corresponding absorbance values are represented by the variables A_{blank}, $A_{control}$, and A_{test}, respectively.

2.8. Data analysis

Each test for antimicrobial and antiproliferative activity was carried out in triplicate to confirm reproducibility. Data analysis was conducted using GraphPad Prism software to determine means and standard deviations.

3. Results and Discussion

3.1. Synthesizing negatively charged silver nanoparticles

The preliminary evaluation, as depicted in Fig. 1(a), involved UV-Vis spectroscopy analysis of the precursor $AgNO_3$ solution (Ag), the *T. rosea* flower extract (ExtTr), and a test sample containing $AgNO_3$ with ExtTr (Ag-ExtTr). While the spectra of both the precursor solution and the original extract exhibited no surface plasmon resonance (SPR) band, the spectrum of the synthesized AgNPsTr displayed a notable absorption peak at approximately 447 nm. This outcome is consistent with findings from other studies indicating a distinctive range of AgNPs typically within 390 to 470 nm [22]. In a study using *Andrographis paniculata* leaf extract to synthesize AgNPs, the AgNPs formation was also confirmed by the appearance of an SPR peak at a wavelength of around 450 nm [23]. In a previous study by Chafidz et al., the formation of AgNPs from *banana raja* peel extract was also confirmed, corresponding to an SPR value of 450 nm [24]. As a result, the successful creation of AgNPsTr using the specified methodology can be affirmed. These initial findings will be the foundational groundwork for subsequent experiments, exploring various operational parameters and their effects on the synthesized AgNPsTr.

The investigation aimed to determine the optimal concentration of the *T. rosea* flower extract, spanning from 0.6 to 1.8 g L^{-1} with the results as presented in Fig. 1(b). At a low concentration of 0.6 g L^{-1}, any pronounced peak was absent within the specified range, signifying a limited formation of AgNPsTr. As the concentration increased, the absorption peak at approximately 440 nm exhibited a heightened intensity, measuring 0.298, 0.378, and 0.420 in correspondence to the concentrations of 0.9, 1.2, and 1.5 g L^{-1} of the *T. rosea* flower extract. Nevertheless, the *T. rosea* flower extract concentration reached 1.8 g L^{-1}, and the observed signal demonstrated a marginal increment, registering at 0.435. This observation established a link between extract concentration and AgNPsTr formation, revealing higher yields at elevated concentrations. However, formation efficiency peaked with the increased extract concentration, leading to larger nanoparticles, indicating a saturation point [25,26]. These findings led to the determination that the most effective concentration of flower extract for synthesizing AgNPsTr was 1.5 g L^{-1}.

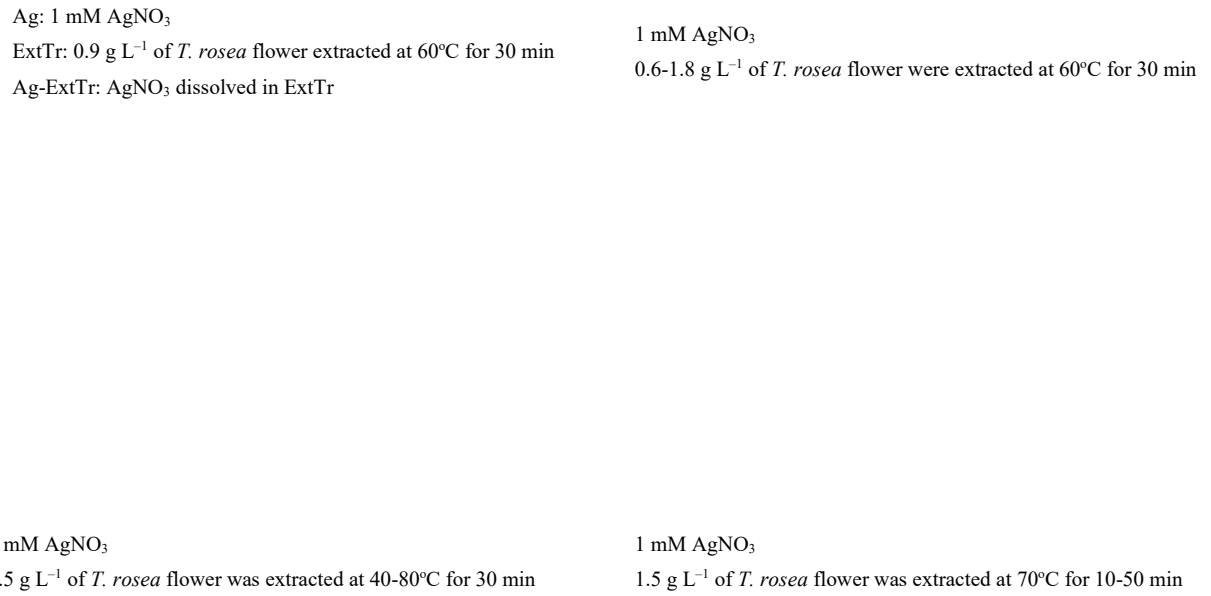

Fig. 1. UV-Vis spectroscopy analysis of the synthesized samples forming AgNPs-Neg

Throughout the extraction procedure, a consistent temperature was maintained within the system. Varied extraction temperature ranges, spanning from 40 to 80°C, were employed to investigate its impact on the process. Fig.

1(c) illustrates the progressive increase in sample absorption at the specified wavelength as the temperature gradually rose. As temperatures escalated, the efficacy of extracting chemical components from plants displayed a marked enhancement [27]. Optimal efficiency was achieved at 70°C, as shown by the highest value in absorption peak, while a decline in absorbance was observed at 80°C. This observation underscored the susceptibility of necessary extract components for AgNPsTr generation to decomposition under excessive heat, leading to diminished overall process efficiency [28]. As a result, a judicious application of moderate heat at 70°C is recommended for optimal AgNPsTr formation.

In the pursuit of optimizing the AgNPsTr formation within the *T. rosea* flower extract, the duration of extraction emerged as a critical factor that determined the process. Fig. 1(d) visualizes the outcomes obtained from various extraction periods, spanning 10 to 50 min. With an extended extraction duration, a discernible enhancement in AgNPsTr generation was observed, as proven by the increasing absorbance levels. This progression in absorbance, nevertheless, reached a saturation point beyond the 40-minute extraction. It became obvious that the extraction efficiency improved within a specific timeframe as the duration increased. This improvement plateaued after extracting reached 40 min, implying that beyond this threshold, further time did not significantly impact extraction efficiency. This phenomenon implies that once equilibrium is established between the solute inside and outside the *T. rosea* flower powder, additional time can insignificantly determine the extraction process [29]. For this reason, the optimal duration for extracting the *T. rosea* flower powder, fostering the most favorable synthesis of AgNPsTr, was determined to be 40 min.

Following a comprehensive experimentation, the most favorable conditions for the formation of AgNPsTr were determined to involve the dissolution of 1 mM $AgNO_3$ within a solution containing 1.5 g L^{-1} of *T. rosea* flower powder, extracted at 70°C for 40 min. Subsequently, zeta potential measurements were conducted on the synthesized material produced under these precise conditions. The outcomes then revealed a negative zeta potential, thereby designating this synthesized material as AgNPs-Neg.

Fig. 2. The zeta potential analysis of AgNPs-Neg

Specifically, the measured zeta potential of AgNPs-Neg was registered at –24.8 mV (Fig. 2). This recorded zeta potential indicated a moderate stability level for AgNPs-Neg, as particles exhibiting positive or negative values around or surpassing ±30 mV are generally acknowledged to induce stable dispersion. Furthermore, the zeta potential of metallic nanoparticles is predominantly determined by the presence of capping agents [30]. The negative zeta potential observed in AgNPs-Neg should be linked to the presence of carbohydrates, quinones, flavonoids, and phenolic compounds within the *T. rosea* flower extract. This finding aligns with the previous research conducted on AgNPs synthesized using the *Tabebuia rosea* leaf extract [20].

3.2. Synthesizing neutrally and positively charged silver nanoparticles

Building upon the groundwork established with AgNPs-Neg, the research pursued the development of AgNPsTr materials featuring positive and neutral zeta potentials. To achieve this, the varying concentrations of chitosan were introduced during synthesis, leveraging its stabilizing capacity and the positively charged $-NH_3^+$ fragments [31].

The introduction of chitosan, as shown in Fig. 3, induced a notable blueshift in the UV-Vis absorption spectrum. Previously observed at approximately 447 nm, the absorption peaks exhibited a decremental trend to 419, 414, 409, and 407 nm, corresponding to the chitosan concentrations of 0.08, 0.16, 0.24, and 0.32%, respectively. The blueshift observed in the UV-Vis spectrum during nanoparticle synthesis suggests the potential formation of smaller nanoparticles [32, 33]. This phenomenon underscores the efficacy of chitosan as an adept capping agent, facilitating the stabilization of nanoparticles at their original smaller sizes. Substantiating this effect is the notably elevated absorbance of AgNPsTr in chitosan-present samples, recording approximately 1.3 times higher than those devoid of chitosan. The stabilizing influence of this agent effectively forestalled nanoparticle aggregation, culminating in a heightened nanoparticle concentration observed at lower wavelengths [34].

Fig. 3. UV-Vis spectroscopy analysis of AgNPsTr synthesized at varied chitosan concentrations

As depicted in Fig. 4, the evaluation of zeta potential, while utilizing chitosan, was carried out for every sample. A clear trend emerged: as the concentration of chitosan increased, the potential values progressively shifted towards the positive spectrum, revealing an upward trajectory. The pinnacle of this trend manifested at +24.9 mV with a chitosan concentration of 0.32%. However, the increase in zeta

potential of AgNPsTr was negligible from chitosan concentrations from 0.16 to 0.32%. Moreover, the surface plasmon resonance blueshifted at 419, 414, 409, and 407 nm corresponding to 0.08, 0.16, 0.24, and 0.32%Ch. The AgNPsTr sample treated with 0.24% chitosan was classified as AgNPs-Pos, exhibiting an acceptable zeta potential. The augmentation in chitosan concentration correlated with a rise in positive fragments, surpassing the prevalence of negative fragments sourced from the *T. rosea* flower extract [16]. Simultaneously, the recorded peak exhibited an increased definition, indicating superior monodispersion and uniformity in particle size [35]. This enhancement stemmed from robust electrostatic interactions fostered by chitosan, resulting in heightened particle homogeneity.

From the zeta potential results, a trendline was constructed to determine the zero point for synthesizing AgNPs with a neutral potential, designated as AgNPs-Neu. As depicted in Fig. 5(a), the introduction of chitosan into a chitosan-free sample led to a notable elevation in potential. The estimated zero point for achieving neutrality was approximately 0.04% of chitosan. Subsequently, the estimated value was employed to synthesize AgNPs-Neu, which was then compared with AgNPs-Neg and AgNPs-Pos as presented in Fig. 5(b). When compared to AgNPs-Neg, both AgNPs-Pos and AgNPs-Neu displayed a blueshift in their absorption wavelengths. However, the shift observed in AgNPs-Pos was slightly smaller, likely attributable to the lower concentration of chitosan utilized in the treatment. Despite AgNPs-Neu showing a lower absorption peak than AgNPs-Pos, the variance observed was insignificant, reaffirming the established stabilizing effect of chitosan.

Fig. 4. Investigating the influence of chitosan concentration on the zeta potential in AgNPs-Pos synthesis: 0.08% chitosan (a), 0.16% chitosan (b), 0.24% chitosan (c), and 0.32% chitosan (d)

Fig. 5. Evaluation of chitosan concentration in AgNPs-Neu synthesis: Dependence of zeta potential on chitosan concentration (a) and UV-Vis of AgNPs-Neg, AgNPs-Neu, and AgNPs-Pos (b)

Table 1. The concentration of Ag^+ and AgNPsTr from ICP-OES measurement

Samples	Concentration of Ag^+ (mg L^{-1})	Reaction efficiency (%)	Concentration of AgNPsTr (mg L^{-1})
$AgNO_3$	68.6		
AgNPs-Neg	27.3	60.2	41.3
AgNPs-Neu	12.4	81.9	56.2
AgNPs-Pos	10.9	84.1	57.7

Under the conditions optimized for the experiment, the bio-synthesized samples of AgNPs-Neg, AgNPs-Neu, and AgNPs-Pos underwent an analysis by means of ICP-OES. The findings, as depicted in Table 1, affirmed the successful synthesis of AgNPs-Neu and AgNPs-Pos, demonstrating the high efficiencies of 81.9 and 84.1%, respectively. Whereas, the synthesis of AgNPs-Neg yielded a more modest result, achieving an efficiency of 60.2%. The AgNPsTr concentration presence in the synthesized samples (AgNPs-Neg, AgNPs-Neu, and AgNPs-Pos) using *T. rosea* flower extract were 41.3, 56.2, and 57.7 mg L^{-1}, respectively.

3.3. Characteristics of the synthesized AgNPsTr

Fig. 6 illustrates the XRD patterns of the synthesized AgNPsTr samples characterized by three distinct zeta potential charges. In all three sample patterns, distinct peaks at 2θ angles of 38.13, 44.30, 64.51, and 77.45° were identified, matching the (111), (200), (220), and (311) lattice planes of silver, respectively. These observations align with the diffraction standards as outlined in JCPDS, No. 89-3722 [36]. In particular, the intensity of the (111) peak surpassed that of other planes, indicating that the predominant orientation for the crystal structure of the AgNPsTr samples was the (111) plane. The XRD analysis corroborated the absence of silver oxide phases; it signified the production of pure silver crystalline in the generated AgNPsTr. Based on the findings as presented in Table 2, the average crystallite sizes for the synthesized AgNPsTr were determined as follows: 19.7 nm for AgNPs-Neg, 15.8 nm for AgNPs-Neu, and 14.2 nm for AgNPs-Pos. Outstandingly, AgNPs-Pos exhibited the smallest average size, followed by AgNPs-Neu and AgNPs-Neg, respectively.

Fig. 6. XRD pattern of AgNPs-Neg, AgNPs-Neu, and AgNPs-Pos

As presented in Fig. 7, the efficacy of utilizing *T. rosea* flower extract and chitosan in the synthesis process was elucidated more through FTIR analysis. This analysis encompassed the original *T. rosea* flower extract, pure chitosan, and the resulting spectra of three distinct AgNPsTr samples: AgNPs-Neg, AgNPs-Neu, and AgNPs-Pos. The spectra of the *T. rosea* flower extract showed a broad band in the range of 3650-3050 cm^{-1}, indicative of O–H stretching vibrations stemming from hydroxyl groups present in carbohydrates and phenolic compounds. Additionally, distinct peaks within the 1650-1300 cm^{-1} region confirmed the existence of quinones and flavonoids, characterized by –C=O groups and aromatic rings [37]. Particularly, these signature signals were consistently observed in the spectra of all three AgNPsTr samples, affirming the retention of these compounds on the surface of the as-prepared materials.

Simultaneously, the chitosan spectra revealed a distinct profile, notably displaying a broad asymmetric band between 3600 and 3100 cm^{-1}, encompassing the overlapped O–H and N–H stretching vibrations [38]. Specific peaks at 1630 cm^{-1} and 1380 cm^{-1} indicated C=O stretching in amide I and C–N stretching in amide III, while the presence of C–O stretching was evident at 1065 cm^{-1} [39]. Obviously, these characteristic signals were absent in the spectrum of AgNPs-Neg but appeared prominently in AgNPs-Neu and AgNPs-Pos. This analysis confirmed a pivotal role of the *T. rosea* flower extract and chitosan as the effective capping agents in the synthesis of AgNPsTr. Their consistent presence in the spectra of the synthesized nanoparticles underscores their active participation in the synthesis process, further validating their efficacy as stabilizing agents.

The morphological characteristics of the synthesized AgNPsTr were further examined through TEM imaging and the size distribution analysis, as presented in Fig 8. Across all three samples, AgNPsTr were consistently observed to assume a spherical shape. Notably, for AgNPs-Neg, the average particle size measured up to 34.6 nm, exhibiting a deviation of 5.2 nm. This trend indicated that the lack of an effective stabilizer led to particle aggregation and irregular size distribution. In contrast, the introduction of chitosan in AgNPs-Neu demonstrated a marked improvement. The average particle size reduced to 21.7 nm with a smaller deviation of 3.5 nm, highlighting the effective role of chitosan in fostering well-dispersed particles. Furthermore, this trend continued in AgNPs-Pos, showcasing a further decrease in average size to 16.8 nm. However, in this instance, a higher concentration of chitosan resulted in a larger deviation of 5.4 nm; it suggests the formation of a thicker capping layer around the particles, leading to non-uniform sizes.

Fig. 7. FTIR spectra of the prepared samples: ExtTr, Ch, AgNPs-Neg, AgNPs-Neu, and AgNPs-Pos

Table 2. Phase constituents and crystallite dimensions of fabricated AgNPsTr

2θ (°)		38.13	44.30	64.51	77.45
Fw	AgNPs-Neg	0.418	0.520	0.449	0.479
	AgNPs-Neu	0.513	0.697	0.528	0.614
	AgNPs-Pos	0.501	0.704	0.584	0.856
Cry (nm)	AgNPs-Neg	20.1	16.5	20.9	21.3
	AgNPs-Neu	16.4	12.3	17.8	16.6
	AgNPs-Pos	16.8	12.2	16.1	11.9
Average Cry (nm)	AgNPs-Neg	19.7			
	AgNPs-Neu	15.8			
	AgNPs-Pos	14.2			

Fig. 8. TEM images and the size distribution of AgNPs-Neg (a, b), AgNPs-Neu (c, d), and AgNPs-Pos (e, f)

3.4. Antimicrobial profiles of synthesized AgNPsTr

Table 3. IC_{50} values of AgNPsTr against bacterial, fungal, and cancer cell lines

Bacteria/fungi/cancer cells		AgNPs-Neg (mg L^{-1})	AgNPs-Neu (mg L^{-1})	AgNPs-Pos (mg L^{-1})	Control
Negative-gram bacteria	*E. coli*	0.52 ± 0.05	77.32 ± 2.50	14.98 ± 1.15	0.36 ± 0.10
	P. aeruginosa	0.52 ± 0.05	128.80 ± 3.47	20.01 ± 1.44	224.05 ± 7.74
	S. enterica	14.06 ± 1.03	111.04 ± 1.22	34.04 ± 1.81	22.41 ± 2.58
Positive-gram bacteria	*B. subtilis*	30.94 ± 1.55	104.51 ± 4.50	85.48 ± 2.21	186.88 ± 7.74
	L. fermentum	3.64 ± 0.50	115.07 ± 1.87	106.87 ± 3.46	53.17 ± 3.61
	S. aureus	1.03 ± 0.05	117.29 ± 4.12	93.08 ± 2.37	1.03 ± 0.26
Fungi	*C. albican*	7.39 ± 0.50	77.55 ± 3.68	58.28 ± 1.83	68.15 ± 2.58
Cancer cells	A549	214.6 ± 8.6	2001.2 ± 22.3	1439.4 ± 26.3	21.1 ± 1.3
	Hep-G2	256.4 ± 10.9	1458.6 ± 17.3	306.6 ± 14.3	23.3 ± 2.7
	KB	189.1 ± 14.4	1178.6 ± 13.8	495.1 ± 26.6	11.6 ± 0.5
	MCF-7	33.4 ± 0.5	1739.7 ± 14.2	418.8 ± 5.7	23.7 ± 1.5

Fig. 9. Antibacterial (a, b) and anticancer (c) activity of AgNPsTr

To assess their potential applications, three variants of AgNPsTr underwent an evaluation for their biological activities, including antibacterial, and anticancer properties. The effectiveness in inhibiting microorganisms and cancer strains was particularly contingent upon the concentration of the administered AgNPsTr, as demonstrated in Fig. 9.

In the evaluation of antibacterial efficacy, AgNPs-Neg demonstrated robust inhibitory effects against gram-negative bacteria, even at minimal concentrations as low as 2.2 mg L^{-1}. While AgNPs-Pos exhibited satisfactory effectiveness against these strains, its inhibitory effects were comparatively less pronounced than those observed with AgNPs-Neg. in particular, the discernible inhibitory effects of AgNPs-Pos were only evident at higher concentrations, specifically at

35.0 and 140.0 mg L^{-1}. In contrast, AgNPs-Neu manifested a weak inhibitory impact on gram-negative bacteria. When directed towards gram-positive bacteria, overall outcomes were found similar. AgNPs-Neg exhibited substantial inhibitory effects started from a concentration of 8.8 mg L^{-1}, whereas both AgNPs-Pos and AgNPs-Neu displayed comparatively weak efficacy. The divergent outcomes observed across bacterial strains can be attributed to inherent structural disparities within their cell walls. The thicker layer of peptidoglycan in gram-positive bacteria rendered them less susceptible to infiltration and destruction, in contrast to the thinner layer present in gram-negative bacteria [40].

Conventionally, positively charged AgNPsTr demonstrated superior bactericidal activity against various microorganisms, and recent studies investigating negatively charged AgNPsTr derived from plant extract-mediated synthesis attribute this enhanced antibacterial efficacy to the presence of specific molecules. Components such as flavonoids and quinones from the natural extract appear to coat the surface of AgNPsTr, potentially contributing to their heightened antibacterial activity [7,41].

In the evaluation of anticancer activity, AgNPs-Neg emerged as notably effective among the tested cancer strains. At the concentrations exceeding 500 mg L^{-1}, AgNPs-Neg displayed potent inhibitory potential, achieving nearly complete inhibition rates across all cancer cell lines. Concomitantly, AgNPs-Pos demonstrated the significant inhibitory effects, approximately 80%, at concentrations above 2000 mg L^{-1}, albeit generally found lower than AgNPs-Neg. In contrast, AgNPs-Neu exhibited comparatively lower inhibitory effects across diverse cancer strains. The findings affirmed AgNPs-Neg's superior and consistent anticancer activity, while AgNPs-Neu and AgNPs-Pos displayed varying efficacy levels with AgNPs-Pos showcasing intermediate inhibitory effects. These outcomes align with earlier discussions on AgNPsTr's antibacterial and antifungal activities. The IC_{50} values, derived from the illustrated graph and depicted in Table 3, confirmed earlier discussions regarding the effectiveness of different AgNPsTr variants. AgNPs-Neg exhibited significantly lower IC_{50} values when combating fungal and bacterial strains as well as cancer cells compared to AgNPs-Neu and AgNPs-Pos, underscoring its superior efficacy against these microorganisms.

According to Menichetti, the antibacterial activity of AgNPs is determined by various factors, including shape, size, charge, and surface stabilizer [42]. For instance, the size of AgNPs is a critical determinant of their antimicrobial effectiveness. Smaller particles possess a larger surface area compared to the larger ones, potentially enhancing their bactericidal behavior [43]. The shape of AgNPs also plays a significant role in their antimicrobial activity. Spherical AgNPs were found more effective against bacteria than rod-shaped particles [44]. Regarding charge, the observed impact on bactericidal activity varied. Positively charged AgNPs exhibited the highest bactericidal activity against bacteria, while negatively charged AgNPs displayed the least activity. Neutrally charged AgNPs showed an intermediate antibacterial activity [7]. Furthermore, the electrostatic attraction between nanoparticles and bacterial cells has been shown to be a principal characteristic of antimicrobial activity [45]. The surface stabilizer of AgNPs has been recognized to significantly influence their antibacterial activity. Stabilizing compounds present in the plant extracts enhanced the antibiotic activity better than chemical stabilizers [46,47]. The mechanisms of microbial death caused by AgNPs can occur through various pathways. Commonly, four well-documented antibacterial effects of AgNPs include (i) attachment to the surface of microbial membranes, (ii) disruption of cellular biomolecules upon internalization into bacterial cells, leading to intracellular damage, (iii) induction of cellular toxicity through the generation of reactive oxygen species (ROS), causing oxidative stress within the cell, and (iv) interference with the cell's signal transduction pathways [48]. Fig. 10 illustrates the antimicrobial mechanism of AgNPs. It can be observed that the particle size and the electrostatic interaction between AgNPs and the microbial membrane are two factors that significantly influence the antimicrobial activity of AgNPs [49]. From the results of the present work, a relationship among antimicrobial activity, stabilizers, particle size, and particle charge emerged. In particular, the presence of stabilizers appeared to outweigh the impact of particle size and surface charge. Remarkably, AgNPs-Neg, despite having the largest particle size, exhibited an enhanced antibiotic activity due to the presence of flavonoids and phenolics. AgNPs-Pos also displayed better microbial inhibition compared to AgNPs-Neu, attributed to their smaller particle size. Finally, the influence of nanoparticle surface charge on antimicrobial activity seems to be relatively weaker.

Fig. 10. A primary mechanism illustrating the antimicrobial activity of AgNPs

Table 4. A comparison to the present work with other studies synthesized the positive-charged AgNPs

Charge of AgNPs	Reductant/Stabilizer	Shape/Size/Zeta potential	Antimicrobial activity	Reference
Negative	$NaBH_4$/$NaBH_4$	Spherical/8 nm/–38 mV	- Bacteria: *Staphylococcus aureus, Streptococcus mutans, Streptococcus pyogenes, Escherichia coli, Proteus vulgaris*.	[7]
Neutral	Starch/Starch	Spherical/10 nm		
Positive	$NaBH_4$/[C_{12}mim][Cl]	Spherical/9 nm/+50 mV	- Activity order: Positive > neutral > negative.	
Positive	$NaBH_4$/[C_{12}mim][Cl]	Spherical/6 nm/+50 mV	- Bacteria: *Staphylococcus aureus, Bacillus subtilis, Escherichia coli, Salmonella* typhi. Fungi: *Candida albicans*. Cancer cell: Hep-G2. - Activity order: [C_{12}mpy]AgNPs > [C_{12}mim]AgNPs > [C_{18}mpy]AgNPs > [C_{18}mpy]AgNPs.	[50]
	$NaBH_4$/[C_{18}mim][Cl]	Spherical/2 nm/+58 mV		
	$NaBH_4$/[C_{12}mpy][Cl]	Spherical/4 nm/+25 mV		
	$NaBH_4$/[C_{18}mpy][Cl]	Spherical/2 nm/+58 mV		
Negative	$NaBH_4$/Citrate	Spherical/45 nm/–30 mV	- Bacteria: *Escherichia coli*.	[12]
Positive	$NaBH_4$/ethyleneimine	Spherical/6 nm/+42 mV	- Activity order: Positive > negative.	
Negative	*Prunus cerasus* leaf extract	Spherical/32 nm/–7 mV	- Bacteria: *Escherichia coli, Enterococcus faecalis, Klebsiella pneumonia, Staphylococcus aureus*.	[51]
Positive	*Prunus cerasus* leaf extract/Chitosan	Spherical/50 nm/+9 mV	- Activity order: Positive > negative.	
Negative	*Tabebuia rosea* flower extract	Spherical/35 nm/–25 mV	- Bacteria: *Pseudomonas aeruginosa, Escherichia coli*, *Salmonella enterica*, *Bacillus subtilis*, *Lactobacillus fermentum*, *Staphylococcus aureus*. Fungi: *Candida albicans*. Cancer cells: A549, Hep-G2, KB, MCF-7. - Activity order: Negative > positive > neutral.	This work
Neutral	*Tabebuia rosea* flower extract/Chitosan	Spherical/22 nm		
Positive	*Tabebuia rosea* flower extract/Chitosan	Spherical/17 nm/+23 mV		

[C_{12}mim][Cl]: 1-dodecyl-3-methylimidazolium chloride
[C_{18}mim][Cl]: 1-octadecyl-3-methylimidazolium chloride
[C_{12}mpy][Cl]: 1-dodecyl-3-methylpyridinium chloride
[C_{18}mpy[Cl]: 1-octadecyl-3-methylpyridinium chloride

Table 4 presents a comparison of the synthesis, characteristics, and antimicrobial activity between differently charged AgNPs from previous studies and AgNPsTr from the current study. Research on positive- and neutral-charged AgNPs remains limited, particularly regarding their impact on a biological activity. Traditionally, the positively charged AgNPs in previous studies presented a spherical shape with particle sizes extending from 2 to 50 nm. Several consistent characteristics were observed in prior research including: (i) surface charge emerged as a pivotal factor determining the inhibitory activity of the synthesized AgNPs; (ii) positively charged AgNPs displayed a higher inhibitory activity against bacteria, fungi, or cancer cells compared to negatively or neutrally charged counterparts; and (iii) solubility significantly affected the antimicrobial activity of the positively charged AgNPs. However, these studies also possessed a number of limitations. Firstly, they lack a comprehensive evaluation of AgNPs with different surface charges, particularly for the neutral charge group. Most studies focused primarily on the antimicrobial activity of AgNPs, often overlooking other potential characteristics. Many studies have also relied on toxic reducing agents such as $NaBH_4$ for synthesis, rather than utilizing eco-friendly plant extracts. Another limitation is that the factors determining the synthesis process and its efficiency have not been thoroughly assessed. The production of AgNPs with varying charges involves a complex process requiring multiple reducing and stabilizing agents and several steps, which further can complicate the synthesis. In contrast, the current study employed the non-toxic reducing and stabilizing agents with a simpler process. It addressed the existing gaps by exploring the impact of chitosan concentration on zeta potential, the influence of extraction conditions on nanoparticle formation, and synthesis efficiency. Furthermore, the study evaluated the biological activity against bacteria and various cancer cell lines.

4. Conclusion

This study effectively involved *T. rosea* flower extract and chitosan to precisely control the surface charges of the synthesized AgNPsTr. The resulting AgNPsTr demonstrated distinct zeta potentials: –24.8 mV (AgNPs-Neg), +24.9 mV (AgNPs-Pos), and a neutral state (AgNPs-Neu) achieved by incorporating 0.04% chitosan. These charge variations corresponded to the particle sizes of 19.7, 14.2, and 15.8 nm, respectively. In particular, compared to other formulations AgNPs-Neg exhibited superior antimicrobial and anticancer activities, highlighting the critical role of surface stabilizers. Our controlled synthesis method not only highlights avenues for optimizing synthesis parameters but also offers significant implications for expanding biomedical applications. This study provides a foundational understanding of how surface charge, particle size, and stabilizers influence the properties of AgNPs, offering a basis for future research in pharmaceutical and biomedical fields. Additionally, it presents an eco-friendly approach for synthesizing nanospherical silver particles with alterations in particle surface charge from plant extracts and friendly polymers containing amine functional groups. Future research should focus on exploring the specific mechanisms behind the observed antimicrobial and anticancer activities, as well as investigating the long-term stability and biocompatibility of these AgNPs in vivo. Moreover, further studies may explore the scalability of this eco-friendly

synthesis method for industrial applications, such as drug delivery systems or diagnostic tools.

Acknowledgments

This study has been funded in part by the Can Tho University, Code: TSV2023-78.

References

1. M. Abass Sofi, S. Sunitha, M. Ashaq Sofi, S.K. Khadheer Pasha, D. Choi, *An overview of antimicrobial and anticancer potential of silver nanoparticles*, J. King Saud Univ. Sci. 34 (2022) 101791
2. N. Durán, M. Durán, M.B. de Jesus, A.B. Seabra, W.J. Fávaro, G. Nakazato, *Silver nanoparticles: A new view on mechanistic aspects on antimicrobial activity*, Nanomed. Nanotechnol. Biol. Med. 12 (2016) 789-799
3. T. Lan Pham, V. Dat Doan, Q. Le Dang, T. Anh Nguyen, T.L. Huong Nguyen, T.D. Thuy Tran, T.P. Lan Nguyen, T.K. Anh Vo, T. Huy Nguyen, D. Lam Tran, *Stable biogenic silver nanoparticles from Syzygium nervosum bud extract for enhanced catalytic, antibacterial and antifungal properties*, RSC Adv. 13 (2023) 20994-21007
4. N.S. Alharbi, N.S. Alsubhi, *Green synthesis and anticancer activity of silver nanoparticles prepared using fruit extract of Azadirachta indica*, J. Radiat. Res. Appl. Sci. 15 (2022) 335-345
5. S. Jebril, R. Khanfir Ben Jenana, C. Dridi, *Green synthesis of silver nanoparticles using Melia azedarach leaf extract and their antifungal activities: In vitro and in vivo*, Mater. Chem. Phys. 248 (2020) 122898
6. T. Silva, L.R. Pokhrel, B. Dubey, T.M. Tolaymat, K.J. Maier, X. Liu, *Particle size, surface charge and concentration dependent ecotoxicity of three organo-coated silver nanoparticles: comparison between general linear model-predicted and observed toxicity*, Sci. Total Environ. 468-469 (2014) 968-976
7. A. Abbaszadegan, Y. Ghahramani, A. Gholami, B. Hemmateenejad, S. Dorostkar, M. Nabavizadeh, H. Sharghi, *The effect of charge at the surface of silver nanoparticles on antimicrobial activity against gram-positive and gram-negative bacteria: A preliminary study*, J. Nanomater. 2015 (2015) 1-8
8. S.M. Rakib-Uz-Zaman, E. Hoque Apu, M.N. Muntasir, S.A. Mowna, M.G. Khanom, S.S. Jahan, N. Akter, M.A. R. Khan, N.S. Shuborna, S.M. Shams, K. Khan, *Biosynthesis of silver nanoparticles from Cymbopogon citratus leaf extract and evaluation of their antimicrobial properties*, Challenges 13 (2022) 18
9. N.P.U. Nguyen, N.T. Dang, L. Doan, T.T.H. Nguyen, *Synthesis of silver nanoparticles: From conventional to 'modern' methods-A review*, Processes 11 (2023) 2617
10. A. Sharonova, K. Loza, M. Surmeneva, R. Surmenev, O. Prymak, M. Epple, *Synthesis of positively and negatively charged silver nanoparticles and their deposition on the surface of titanium*, IOP Conf. Ser. Mater. Sci. Eng. 116 (2016) 012009
11. K. Ssekatawa, D.K. Byarugaba, C.D. Kato, E.M. Wampande, F. Ejobi, J.L. Nakavuma, M. Maaza, J. Sackey, E. Nxumalo, J.B. Kirabira, *Green strategy-based synthesis of silver nanoparticles for antibacterial applications*, Front. Nanotechnol. 3 (2021) 697303
12. L.R. Pokhrel, Z.L. Jacobs, D. Dikin, S.M. Akula, *Five nanometer size highly positive silver nanoparticles are bactericidal targeting cell wall and adherent fimbriae expression*, Sci. Rep. 12 (2022) 6729
13. A. Gholami, K. Ghezelbash, B. Asheghi, A. Abbaszadegan, A. Amini, *An in Vitro study on the antibacterial effects of chlorhexidine-loaded positively charged silver nanoparticles on Enterococcus faecalis*, J. Nanomater. 2022 (2022) 6405772
14. E. Matras, A. Gorczyca, S.W. Przemieniecki, M. Oćwieja, *Surface properties-dependent antifungal activity of silver nanoparticles*, Sci. Rep. 12 (2022) 18046
15. M.A. Polinarski, A.L.B. Beal, F.E.B. Silva, J. Bernardi-Wenzel, G.R.M. Burin, G.I.B. de Muniz, H.J. Alves, *New perspectives of using chitosan, silver, and chitosan-silver nanoparticles against multidrug-resistant bacteria*, Part. Part. Syst. Charact. 38 (2021) 2100009
16. M. Collado-González, V. Fernández Espín, M.G. Montalbán, R. Pamies, J.G. Hernández Cifre, F.G. Díaz Baños, G. Víllora, J. García de la Torre, *Aggregation behaviour of gold nanoparticles in presence of chitosan*, J. Nanoparticle Res. 17 (2015) 268
17. D. Van Phu, L.A. Quoc, N.N. Duy, N.T.K. Lan, B.D. Du, L.Q. Luan, N.Q. Hien, *Study on antibacterial activity of silver nanoparticles synthesized by gamma irradiation method using different stabilizers*, Nanoscale Res. Lett. 9 (2014) 162
18. L.O. Cinteza, C. Scomoroscenco, S.N. Voicu, C.L. Nistor, S.G. Nitu, B. Trica, M.L. Jecu, C. Petcu, *Chitosan-stabilized Ag nanoparticles with superior biocompatibility and their synergistic antibacterial effect in mixtures with essential oils*, Nanomaterials 8 (2018) 826
19. S. Jadoun, R. Arif, N.K. Jangid, R.K. Meena, *Green synthesis of nanoparticles using plant extracts: A review*, Environ. Chem. Lett. 19 (2021) 355-374
20. F. Jiménez-González, J. Vélez-Gómez, J. Melchor-Moncada, L. Veloza, J. Sepúlveda-Arias, *Antioxidant, anti-inflammatory, and antiproliferative activity of extracts obtained from Tabebuia Rosea (Bertol.) DC*, Pharmacogn. Mag. 14 (2018) 25
21. S. Sirigeri, M. Sv, B. Sl, *Phytochemical analysis and biological activity studies of methanolic extract of Tabebuia rosea seeds*, J. Med. Plants Stud. 9 (2021) 41-46
22. E. Sreelekha, B. George, A. Shyam, N. Sajina, B. Mathew, *A comparative study on the synthesis, characterization, and antioxidant activity of green and chemically synthesized silver nanoparticles*, BioNanoScience 11 (2021) 489-496
23. A. Chafidz, S. Rusdi, I. Nurrahman, A.D. Haryanto Kalista Wibowo, A. Kusmayadi, D.T. Hartanto, *Synthesis of silver (Ag) nano/micro-particles via green process using Andrographis paniculata leaf extract as a bio-reducing agent*, Commun. Sci. Technol. 9 (2024) 199-206
24. A. Chafidz, A.R. Afandi, B.M.S. Rosa, J., P. Hidayat, H. Junaedi, *Production of silver nanoparticles via green method using banana raja peel extract as a reducing agent*, Commun. Sci. Technol. 5 (2020) 112-118
25. M. Khan, M. Khan, S.F. Adil, M.N. Tahir, W. Tremel, H.Z. Alkhathlan, A. Al-Warthan, M.R. Siddiqui, *Green synthesis of silver nanoparticles mediated by Pulicaria glutinosa extract*, Int. J. Nanomedicine 8 (2013) 1507-1516
26. J.L. López-Miranda, M. Vázquez, N. Fletes, R. Esparza, G. Rosas, *Biosynthesis of silver nanoparticles using a Tamarix gallica leaf extract and their antibacterial activity*, Mater. Lett. 176 (2016) 285-289
27. A. Antony, M. Farid, *Effect of temperatures on polyphenols during extraction*, Appl. Sci. 12 (2022) 2107
28. S. Raghunath, S. Budaraju, S.M.T. Gharibzahedi, M. Koubaa, S. Roohinejad, K. Mallikarjunan, *Processing technologies for the extraction of value-added bioactive compounds from tea*, Food Eng. Rev. 15 (2023) 276-308
29. Q.W. Zhang, L.G. Lin, W.C. Ye, *Techniques for extraction and isolation of natural products: A comprehensive review*, Chin. Med. 13 (2018) 20
30. A. Sankhla, R. Sharma, R.S. Yadav, D. Kashyap, S.L. Kothari, S. Kachhwaha, *Biosynthesis and characterization of cadmium sulfide*

nanoparticles-An emphasis of zeta potential behavior due to capping, Mater. Chem. Phys. 170 (2016) 44-51

31. T. Kim, J. Shin, B. An, *Adsorption characteristics for Cu(II) and phosphate in chitosan beads under single and mixed conditions*, Polymers 15 (2023) 421
32. M.M.H. Khalil, E.H. Ismail, K.Z. El-Baghdady, D. Mohamed, *Green synthesis of silver nanoparticles using olive leaf extract and its antibacterial activity*, Arab. J. Chem. 7 (2014) 1131-1139
33. B.S. Avinash, V.S. Chaturmukha, H.S. Jayanna, C.S. Naveen, M.P. Rajeeva, B.M. Harish, S. Suresh, A.R. Lamani, *Effect of particle size on band gap and DC electrical conductivity of TiO_2 nanomaterial*, AIP Conf. Proc. 1728 (2016) 020426
34. Z. Nate, M.J. Moloto, P.K. Mubiayi, P.N. Sibiya, *Green synthesis of chitosan capped silver nanoparticles and their antimicrobial activity*, MRS Adv. 3 (2018) 2505-2517
35. S. Skoglund, J. Hedberg, E. Yunda, A. Godymchuk, E. Blomberg, I. Odnevall Wallinder, *Difficulties and flaws in performing accurate determinations of zeta potentials of metal nanoparticles in complex solutions-Four case studies*, Plos One 12 (2017) 0181735
36. D. Arif, M.B.K. Niazi, N. Ul-Haq, M.N. Anwar, E. Hashmi, *Preparation of antibacterial cotton fabric using chitosan-silver nanoparticles*, Fibers Polym. 16 (2015) 1519-1526
37. M. Krysa, M. Szymańska-Chargot, A. Zdunek, *FT-IR and FT-Raman fingerprints of flavonoids-A review*, Food Chem. 393 (2022) 133430
38. C. Branca, G. D'Angelo, C. Crupi, K. Khouzami, S. Rifici, G. Ruello, U. Wanderlingh, *Role of the OH and NH vibrational groups in polysaccharide-nanocomposite interactions: A FTIR-ATR study on chitosan and chitosan/clay films*, Polymer 99 (2016) 614-622
39. S. Kumari, P. Rath, A. Sri Hari Kumar, T.N. Tiwari, *Extraction and characterization of chitin and chitosan from fishery waste by chemical method*, Environ. Technol. Innov. 3 (2015) 77-85
40. Y.N. Slavin, J. Asnis, U.O. Hafeli, H. Bach, *Metal nanoparticles: understanding the mechanisms behind antibacterial activity*, J. Nanobiotechnology 15 (2017) 65
41. R.P. Illanes Tormena, E.V. Rosa, B.F. Oliveira Mota, J.A. Chaker, C.W. Fagg, D.O. Freire, P.M. Martins, I.C. Rodrigues da Silva, M.H. Sousa, *Evaluation of the antimicrobial activity of silver nanoparticles obtained by microwave-assisted green synthesis using Handroanthus impetiginosus (Mart. ex DC.) Mattos underbark extract*, RSC Adv. 10 (2020) 20676-20681
42. A. Menichetti, A. Mavridi-Printezi, D. Mordini, M. Montalti, *Effect of size, shape and surface functionalization on the antibacterial activity of silver nanoparticles*, J. Funct. Biomater. 14 (2023) 244
43. M. López-Heras, I.G. Theodorou, B.F. Leo, M.P. Ryan, A.E. Porter, *Towards understanding the antibacterial activity of Ag nanoparticles: electron microscopy in the analysis of the materials-biology interface in the lung*, Environ. Sci. Nano 2 (2015) 312-326
44. E.M.P. dos Santos, C.C.B. Martins, J.V. de Oliveira Santos, W.R.C. da Silva, S.B.C. Silva, M.A. Pelagio-Flores, A. Galembeck, I.M.F. Cavalcanti, *Silver nanoparticles-chitosan composites activity against resistant bacteria: tolerance and biofilm inhibition*, J. Nanoparticle Res. 23 (2021) 196
45. Z. Li, J. Ma, J. Ruan, X. Zhuang, *Using positively charged magnetic nanoparticles to capture bacteria at ultralow concentration*, Nanoscale Res. Lett. 14 (2019) 195
46. N. Oulahal, P. Degraeve, *Phenolic-rich plant extracts with antimicrobial activity: An alternative to food preservatives and biocides?*, Front. microbiol. 12 (2022) 753518
47. J.A. Aboyewa, N.R.S. Sibuyi, M. Meyer, O.O. Oguntibeju, *Green synthesis of metallic nanoparticles using some selected medicinal plants from Southern Africa and their biological applications*, Plants 10 (2021) 1929
48. T.C. Dakal, A. Kumar, R.S. Majumdar, V. Yadav, *Mechanistic basis of antimicrobial actions of silver nanoparticles*, Front. Microbiol. 7 (2016) 01831
49. Y.N. Slavin, J. Asnis, U.O. Häfeli, H. Bach, *Metal nanoparticles: understanding the mechanisms behind antibacterial activity*, J. Nanobiotechnol. 15 (2017) 65
50. A. Gholami, M.B. Ghoshoon, P. Ghafari, Y. Ghasemi, *The effect of different positively charged silver nanoparticles against bacteria, fungi and mammalian cell line*, Trends Pharm. Sci. 3 (2017) 135-142
51. S. Shinde, V. Folliero, A. Chianese, C. Zannella, A. De Filippis, L. Rosati, M. Prisco, A. Falanga, A. Mali, M. Galdiero, M. Galdiero, G. Franci, *Synthesis of chitosan-coated silver nanoparticle bioconjugates and their antimicrobial activity against multidrug-resistant bacteria*, Appl. Sci. 11 (2021) 9340